applied sciences

MDPI

Communication

Numerical Study of Mode Conversion between Fundamental Lamb and Rayleigh Waves

Alex Vu [1], Leonard J. Bond [2] and Sunil K. Chakrapani [1,3,*]

[1] Department of Mechanical Engineering, Michigan State University, East Lansing, MI 48824, USA
[2] Department of Aerospace Engineering, Iowa State University, Ames, IA 50011, USA
[3] Department of Electrical and Computer Engineering, Michigan State University, East Lansing, MI 48824, USA
* Correspondence: csk@msu.edu

Abstract: This article reports the findings of a numerical study of mode conversion between fundamental Lamb and Rayleigh waves and vice versa in quarter and half spaces. Fundamental Lamb wave (A_0 and S_0) propagation in a plate attached to a quarter space and the subsequent mode conversion to a Rayleigh wave was studied using finite element analysis. B-Scans show that a beat-like phenomenon can be observed for the R $\rightarrow$ L conversion and a generation length can be observed for the L $\rightarrow$ R conversion. The quarter-space model was also used to study the Rayleigh to Lamb mode conversion. Two hypotheses were developed based on the observed mode conversion efficiencies: (a) the main driving factor of mode conversion between Lamb and Rayleigh waves is the grazing incidence of bulk modes and (b) due to scattering and diffraction, the modes will require a generation length to stabilize in amplitude. Both hypotheses were tested and confirmed using numerical models, including a half-space model to study the diffraction of bulk waves from an incident Lamb wave. The results are of significance for nondestructive evaluation of complex structures where such structural discontinuities exist and it becomes important to understand the fundamental mode conversion phenomenon.

Keywords: Lamb waves; Rayleigh waves; quarter space

Citation: Vu, A.; Bond, L.J.; Chakrapani, S.K. Numerical Study of Mode Conversion between Fundamental Lamb and Rayleigh Waves. *Appl. Sci.* **2023**, *13*, 5613. https://doi.org/10.3390/app13095613

Academic Editor: Bahram Djafari-Rouhani

Received: 5 April 2023
Revised: 26 April 2023
Accepted: 28 April 2023
Published: 1 May 2023

1. Introduction

Mode conversion between different propagating wave types is of interest in several academic communities such as seismology, elastodynamics, structural health monitoring and nondestructive evaluation. Specifically, the conversion of one mode type to another based on interaction with geometric features has been explored extensively. This is of specific interest to the nondestructive evaluation and testing community since geometric discontinuities are potential sources of defects, which eventually need to be characterized. Several researchers have explored the mode conversion between P and SV waves [1–3], guided Lamb waves and P and SV waves [4–6] and P and SV and Rayleigh waves [7–13]. However, analyses for the conversion between Rayleigh- and Lamb-type waves are limited and will be the main focus of this article. Although they both are generated from bulk mode interaction with geometric features, their particle displacement, mode velocity, etc., are different, which make them interesting and of importance. Mode conversion between these waves has been studied typically in the specific case of a Lamb wave interaction with a delamination. This was first shown analytically [14], followed by experimental and numerical results for composite and metallic structures [15,16]. In the case of Lamb mode interaction with a delamination, a large portion of the scattered bulk modes will contribute towards the formation of Lamb modes since the energy is trapped within the plate. A similar Lamb wave interaction with a step will result in energy being trapped within the plate. However, in the case of a plate attached to a half-space or quarter-space, the incident Lamb (in the plate) or Rayleigh (in the half-space) energy can be scattered through the half

or quarter spaces as bulk modes, which has not been explored in the literature. In different but related work, Achenbach et al. [17] showed that an incident Rayleigh wave will be scattered into bulk modes when interacting with a sub-surface horizontal crack. However, the analysis was limited to bulk modes and generation of Lamb modes was not explored.

The main objective of the present work is to understand the mode conversion between Rayleigh and Lamb waves in terms of bulk mode interactions. This will be accomplished using numerical models of examples to unify previous understanding of Lamb and Rayleigh mode conversion into bulk modes and bulk mode conversion into Lamb and Rayleigh waves to explain the conversion between Lamb and Rayleigh waves. Mode conversion efficiencies between L $\rightarrow$ R and R $\rightarrow$ L modes were calculated numerically for a plate attached to a quarter-space. To understand this conversion, the Lamb energy exiting out of the plate was captured using a half-space model. The calculated bulk mode conversion efficiency was then used to explain the L $\rightarrow$ R conversion. Furthermore, numerical time–distance plots were used to investigate the difference between the two conversions.

Most practical applications of Lamb waves in NDT/E and SHM utilize the fundamental symmetric and anti-symmetric modes since they can be generated at lower frequency–thickness products. Therefore, to keep the analysis simple, only the fundamental symmetric and anti-symmetric Lamb modes were considered in this study. It is well known that Lamb waves exhibit dispersion characteristics [1–3], and different modes can be generated due to the fundamental relationships between the excitation frequency and thickness of the plate. As an example, a thin plate (1 mm) was chosen and the frequency of excitation was chosen such that only the fundamental symmetric (S_0) and anti-symmetric (A_0) Lamb modes can be generated, as shown in Figure 1 at 1 MHz-mm for aluminum. The material properties will be presented in the next section.

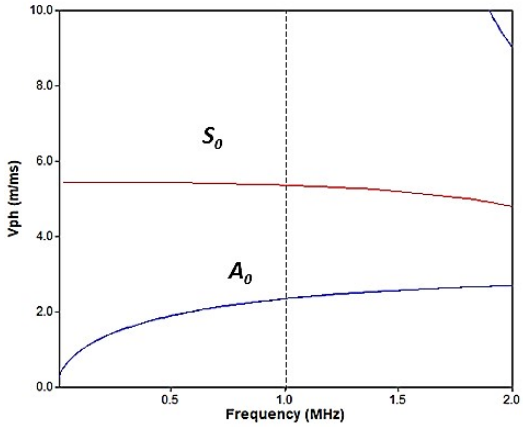

Figure 1. Dispersion curves showing the phase velocity as a function of frequency for a 1 mm plate. The modes of interest are A_0 and S_0 at 1 MHz-mm. The properties of aluminum are E = 69.8 GPa, ν = 0.33, density: ρ = 2700 kg/m^3 and were used to generate the dispersion curve in Disperse software.

2. Numerical Model

The various model geometries used for the wave propagation analysis are shown in Figure 2. Figure 2a,b shows a thin plate (thickness of 1 mm) attached to a quarter space of dimensions 0.5 m X 0.5 m, which will be referred to as the "quarter-space model" throughout this article. Figure 2c shows a thin plate attached to a half space, which will be referred to as the "half-space model". The quarter-space model has a discontinuity D_1, which is defined as the point where the abrupt transition in thickness occurs. The thickness transition plane in which the discontinuity occurs is termed as the discontinuity face. The half-space model has two discontinuities, D_1 and D_2, as shown in Figure 2c. The finite element model was constrained at the bottom of the thick plate (half-space) with fixed boundary conditions, and all other faces were given traction free boundary

conditions to satisfy guided wave propagation as shown in the schematic. The model was meshed using 2D, 8 node quadrilateral elements with a quadratic shape function and plane strain conditions. For convergence of a numerical solution, it is important to have at least 10 elements per wavelength of a specific mode. The present work considers the following modes with their respective velocities: A_0 : 2335 m/s, S_0 : 5346 m/s and R : 2865 m/s. The present work considers narrow-band 1 MHz excitation; therefore, the wavelengths will be A_0 : 2.335 mm, S_0 : 5.346 mm and R : 2.865 mm. Considering the lowest mode wavelength (2.335 mm) and the highest frequency of interest (1 MHz), we require the element size to be 0.23 mm. The final element size chosen for the study such that it captures all the modes was 0.0833 mm. The number of elements near the 90° corner of the quarter-space and half-space models was increased to model the sharp discontinuity.

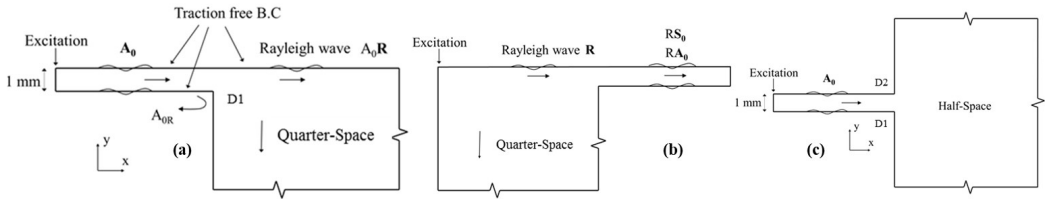

Figure 2. Schematics showing (**a**) quarter-space configuration with thin plate attached used for Lamb to Rayleigh mode study, (**b**) quarter-space with thin plate used for Rayleigh to Lamb mode study and (**c**) half-space model with thin plate attached for bulk mode study.

The equation of motion is given by:

$$[M]\{\ddot{u}\} + [C]\{\dot{u}\} + [K]\{u\} = \{F(t)\} \quad (1)$$

where M is the mass matrix, C is the damping matrix and K is the stiffness matrix. $\ddot{u}$, $\dot{u}$ and u are the nodal acceleration, velocity and displacement vectors, respectively, and $F(t)$ is the load vector. The elemental stiffness matrix was obtained by using the elastic properties of aluminum, E = 69.8 GPa and ν = 0.33, and the mass matrix was obtained using the density ρ = 2700 kg/m^3. For the present case, the damping matrix was set to 0. The load vector is the excitation source and is a function of time for the transient analysis. This was modeled using a 1MHz, 7-cycle sinusoidal toneburst subjected to a Hanning window as shown in Figure 3a. Time integration was performed using Newmark's time integration scheme [18], with an integration time of 50 nanoseconds and a total simulation time of 50 microseconds. The integration time step was chosen such that it satisfies the Nyquist criteria. The finite element problem was solved in ANSYS using a direct sparse solver. Due to the enormous size of the model, graphic processing unit (GPU) acceleration using a Tesla C2075 [19] was utilized. Additionally, the double precision computation and error correcting code of the Tesla were retained to improve simulation accuracy [19]. Selective mode generation of Lamb waves was achieved by applying U_y (for A_0 mode) and U_x (for S_0 mode) nodal displacements along the vertical edge of the plate, as shown in Figure 2. The nodal displacement amplitude determined as a function of time shows the disturbance as it propagates along the plate. An A-scan of the U_y displacement as a function of time determined in the plate before the discontinuity is shown in Figure 3b. Both the excited A_0 mode and the reflected modes from the discontinuity can be observed in the A-Scan. Additionally, displacement profiles or mode shapes were obtained by extracting the U_x and U_y amplitudes along the thickness or depth for a specific time step when the wave propagates across the node.

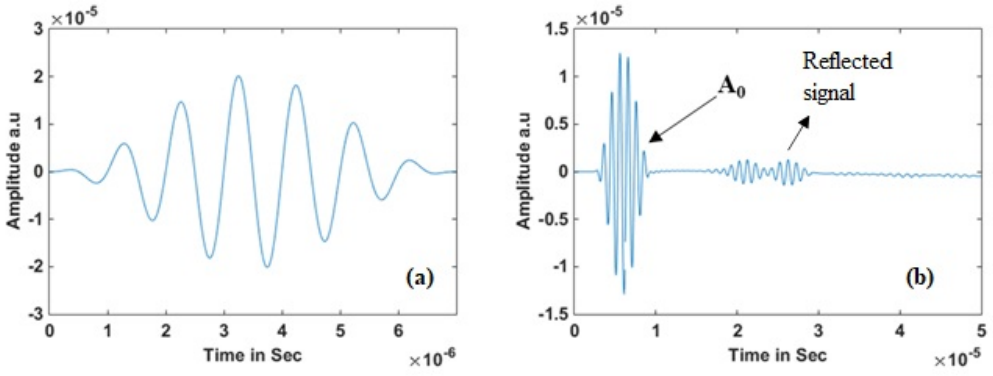

Figure 3. (**a**) The input pulse used for excitation, (**b**) example A-Scan showing the A_0 and reflected disturbance in the time domain.

3. Results

It is convenient to study the mode conversion phenomenon in terms of transmission and reflection coefficients, which will be a measure of the mode conversion efficiency. The time averaged power flow for a propagating mode is given by [1]:

$$P = \frac{1}{t}\int_0^t \int^{D_i} \left[\sigma_{xx}(\dot{U}_x) + \sigma_{xy}(\dot{U}_y)\right] dydt \tag{2}$$

where σ_{xx} and σ_{xy} are the axial and shear stress, respectively, and $\dot{U}_x$ and $\dot{U}_y$ are the particle velocities. The integration is performed over the section D_i, for which the Lamb modes correspond to the thickness of the plate, i.e., $-h/2$ to $h/2$. For Rayleigh waves, the integration was performed from the surface of the quarter space to a depth corresponding to $1.5 \times \lambda_R$ [20]. The transmission coefficient, otherwise termed as conversion efficiency, and reflection coefficients were calculated using [21]:

$$T_c = P_t/P_i, \quad R_c = P_r/P_i \tag{3}$$

where (P_i) is the incident power, (P_t) is the transmitted power and (P_r) is the reflected power. Using the transmission and reflection coefficients, one can use the power flux balance [17,21], $T_c + R_c + P_s = 1$, to obtain the scattering power coefficient (P_s). Similarly, the power flow for the bulk modes, the longitudinal (P) and shear (SV) waves, were obtained using the 1st and 2nd terms of Equation (2) [1].

3.1. Lamb Wave to Rayleigh Wave Conversion

3.1.1. Incident A_0 Mode

A numerical visualization of the nodal displacement vectors for the wave propagation for an incident A_0 mode is shown in Figure 4a. The A_0 mode excited in the thin plate propagates and interacts with the discontinuity D_1, where part of the energy is reflected as A_{0r} and S_{0r} and part of it is transmitted into the quarter-space, where it mode converts into the Rayleigh mode A_0R. When the A_0 mode interacts with D_1, it also gives rise to circular P and SV wave fronts radiating through the quarter-space, as shown in Figure 4a. Furthermore, the SV wave front amplitude is at a maximum in a "shear window", and there is a phase reversal at the center of the window. Such a radiation pattern has been shown previously for a vertical line load acting on top of a half-space [22]. The power coefficients were calculated using Equation (3) and plotted in Figure 4b. The results show that >50% of the incident A_0 energy is scattered, but 34% is converted into the R mode. The reflected energies in the plate are Lamb modes, A_{0R} and S_{0R}, the transmitted Rayleigh mode in the half-space is A_0R and the scattered modes are P_s. Additionally, another R wave can be seen propagating along the vertical edge of the quarter space. By definition of the scattering power coefficient, this additional wave will be included in the power coefficient analysis.

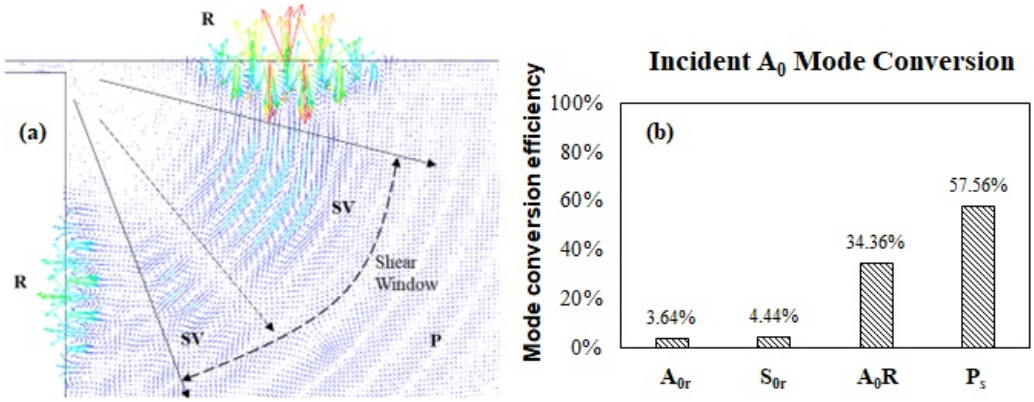

Figure 4. Lamb to Rayleigh mode conversion for an incident A_0 mode: (**a**) snapshot showing the vector plot of total displacement in the quarter-space configuration. P and SV refer to the longitudinal and shear waves, respectively, and R is the Rayleigh wave. (**b**) Mode conversion efficiency of the different modes.

3.1.2. Incident S_0 Mode

The nodal displacement vectors for the S_0 mode interaction with discontinuity are shown in Figure 5a. Unlike the A_0 case, the P waves have a higher amplitude compared to SV, and a distinct shear window (with phase reversal) is not observed. Interestingly, a sub-surface longitudinal wave can be seen propagating ahead of the R wave on the top surface. The mode conversion efficiencies calculated from the numerical model are presented in Figure 5b. About 0.37% of the incident S_0 mode is reflected in the thin plate as an S_0 mode, and less than 0.1% is reflected as an A_0 mode. The Rayleigh mode conversion efficiency for the $S_0 \rightarrow R$ mode was calculated to be 1.19%, which is very small compared to the $A_0 \rightarrow R$ mode conversion efficiency. Once again, using the power flux balance, P_s was calculated to be 98.44%. Additionally, a sub-surface longitudinal wave was also observed, as shown in Figure 5a.

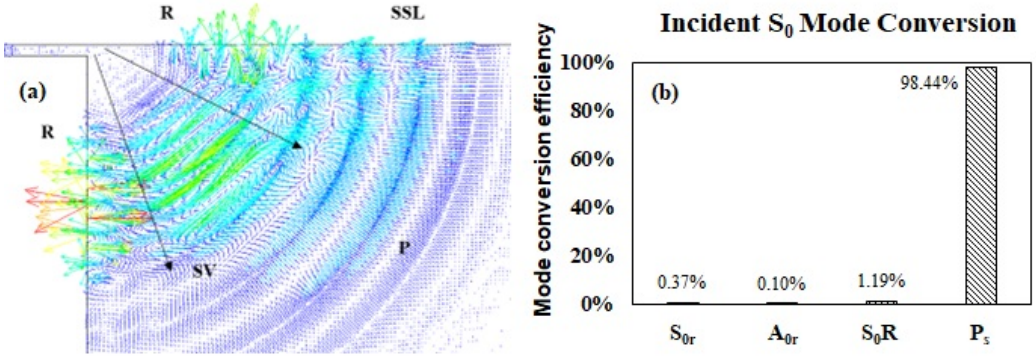

Figure 5. Lamb to Rayleigh mode conversion for an incident S_0 mode: (**a**) snapshot showing the vector plot of total displacement in the quarter-space configuration. P and SV refer to the longitudinal and shear waves, respectively, R is the Rayleigh wave and SSL is the sub-surface longitudinal wave. (**b**) Bar plot for percentages of converted modes.

3.2. Rayleigh to Lamb Wave Conversion

The Rayleigh wave interaction with the discontinuity is shown in Figure 6a. Although the Rayleigh wave was travelling towards the right-hand side, the bulk wave diffracted energy from the discontinuity can be seen travelling in the opposite direction. Both P and SV waves are generated from the mode conversion and propagate though the half space at angles nominally similar to what was observed for the incident A_0 mode case. The mode conversion efficiencies are plotted in Figure 6b and show that >50% of the incident energy is scattered away. Interestingly, the $R \rightarrow S_0$ conversion is higher than the $R \rightarrow A_0$.

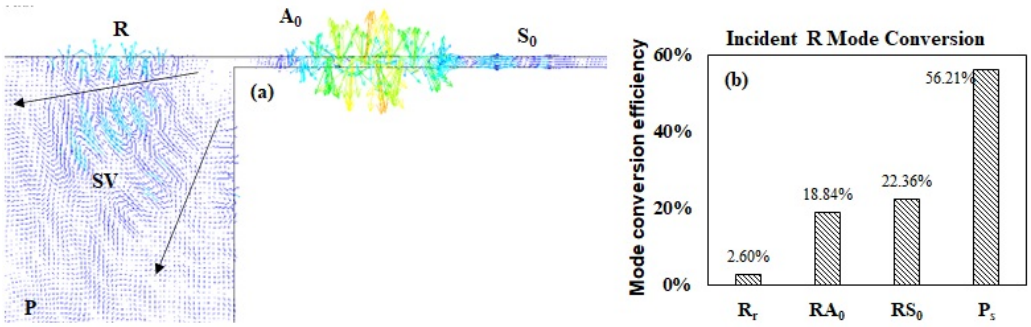

Figure 6. Rayleigh to Lamb mode conversion: (**a**) snapshot showing the vector plot of the total displacement in the quarter-space configuration. P and SV refer to the longitudinal and shear waves, respectively, and R is the Rayleigh wave. (**b**) Bar plot for percentages of converted modes.

4. Discussion

One of the objectives of the present work is to understand the physical mode conversion phenomenon using numerical analysis rather than an analytical expression, which cannot capture the complete scattering behavior. For the case of Lamb to Rayleigh conversion, the energy exiting the plate can be treated at the discontinuity plane as a set of Huygens' sources as shown in Figure 7a. These can act as line or point sources depending on several factors such as the number of sources, the width of sources, the frequency, etc. Due to the complexity of deriving an analytical solution for buried sources in a quarter space, for simplicity, let us neglect the vertical edge of the quarter space and treat it as a half space. This gives rise to two hypotheses: (a) the sources closest to the surface will result in grazing incidence of bulk modes at the top stress-free boundary, and (b) the other sources will result in diffracted bulk waves whose incident angles and phase will result in a "generation length" for the Rayleigh wave.

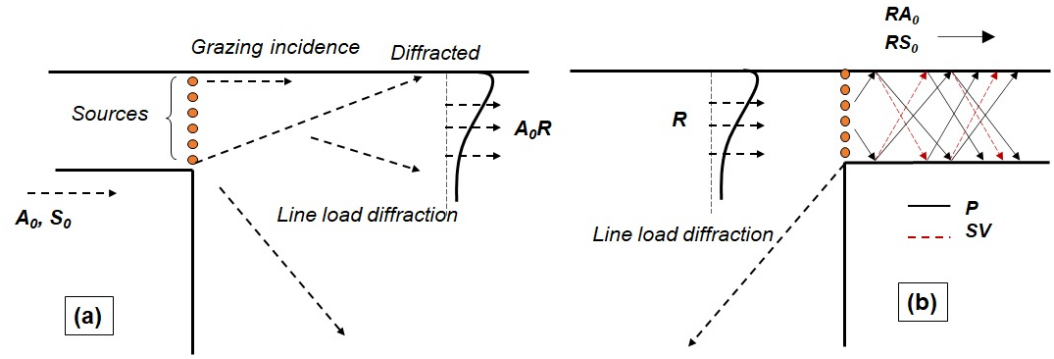

Figure 7. Schematic showing the hypotheses of (**a**) Lamb to Rayleigh mode conversions and (**b**) Rayleigh to Lamb mode conversion. The diffraction will be similar to a line load source with a set of Huygens' sources. This may give rise to two hypotheses: mode conversion of Lamb to Rayleigh via grazing incidence of bulk modes on the half-space and direct diffraction of bulk modes.

Grazing incidence: First, we test the hypothesis of grazing incidence to generate Rayleigh waves. Goodier and Bishop [23] showed that for the case of grazing incidence of bulk waves at a stress-free boundary, the nature of the bulk mode (P vs. SV) will dictate the mode conversion phenomenon. For the case of a grazing incident SV wave, a wave with an exponentially decaying component in the depth direction and an SV wave with a linearly increasing amplitude will be generated. For the case of a grazing incident P wave, the plane wave solutions show that an SV wave is generated along with a P wave travelling with a linearly increasing amplitude. The derivations of these conditions can be found in [3,23]. The exponentially decaying wave forms the basis for Rayleigh wave generation and the linearly increasing amplitude waves are not physically admissible. To place this in the context of the present work, it is necessary to study the energy exiting the plate by

capturing the bulk mode conversions. Instead of using a free-space model, a symmetric half space, as shown in Figure 2c, can be used to capture the radiation. The energy exiting the plate at 90° to the discontinuity into the half space was captured at the receiver point *X* as shown in Figure 8 and used to calculate the mode conversion efficiencies. For an incident A_0 mode as shown in Figure 8a, the conversion to P waves was <0.001%, whereas 33.23% was converted into SV waves. In the case of an incident S_0 mode as shown in Figure 8b, 3.43% was converted into P waves and <0.001% was converted into SV waves. Combing the analytical solution from Goodier and Bishop [23] with the above-measured conversion efficiencies, it can be observed that an incident A_0 mode will mode convert predominantly into SV waves, as shown in Figure 7b, which will further mode convert into Rayleigh waves. The $A_0 \rightarrow$ SV and $A_0 \rightarrow$ R was $\approx$ 34% (Figure 4b), which suggests that the grazing incidence of the SV mode could be the main factor for mode conversion between A_0 and R modes. For the case of the S_0 mode, as shown in Figure 7b, the S_0 will mode convert into P waves and further into Rayleigh waves. However, the $S_0 \rightarrow$ P is 3.43% and $S_0 \rightarrow$ R is only 1% (Figure 5b). Based on the analytical solution for grazing waves, only SV can give rise to exponentially decaying waves. This suggests that for the case of the S_0 mode, $S_0 \rightarrow$ P $\rightarrow$ SV $\rightarrow$ R will be the sequence of mode conversions, which agrees well with the low mode conversion efficiency of S_0.

Moving onto the case of Rayleigh to Lamb wave conversion, it is apparent that the Rayleigh wave will simply act like a line load on the side of the plate. However, the Rayleigh amplitudes decay exponentially with depth; therefore, the excitation of the line load will also vary with plate depth. For the cases considered here, the Rayleigh waves will mode convert to bulk waves in the plate, whose wavelength is significantly larger than the plate thickness. The generation of Lamb waves from bulk wave interactions is well documented in the literature [1–3], particularly the partial wave technique. This technique uses the principle of superposition of three upward and three downward propagating waves to satisfy the stress-free boundary condition used to describe Lamb wave propagation. The reconstructions of the reflected waves or transverse resonances eventually give rise to a guided Lamb mode [2]. This applies very well to the present geometry, where the incident Rayleigh wave will be scattered as bulk modes into the plate structure and subsequently develop into a Lamb wave, as shown in Figure 7.

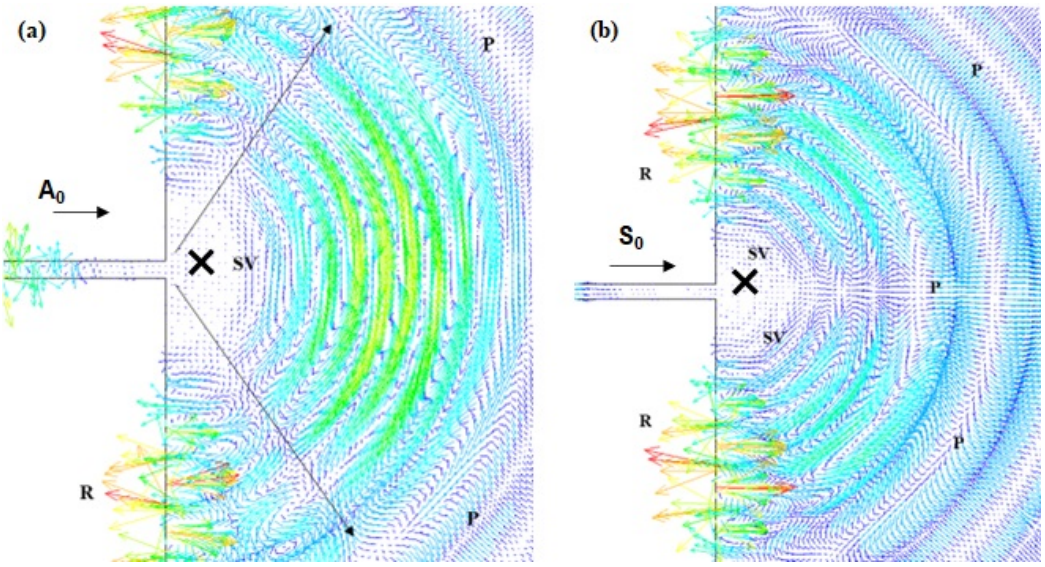

Figure 8. Snapshot showing vector plots of the total displacement in a half-space configuration: (**a**) for an incident A_0 mode and (**b**) for an incident S_0 mode.

Generation length: To test the second hypothesis, i.e., generation length for Rayleigh and Lamb modes, a numerical line scan was carried out. The starting point of the line scan was chosen such that it was 10 mm from the discontinuity, and surface A-Scans (displacement as

a function of time) were extracted at 0.2 mm increments for up to 40 mm from the starting point. The Hilbert transform was used to obtain an analysis of each A-Scan, and finally a Hilbert line scan was obtained as shown in Figure 9. The location of the discontinuity (10 mm from start point) is marked in dashed lines in Figure 9. The numerical Uy line scan of the $A_0 \rightarrow R$ conversion is shown in Figure 9a. It can be noticed that after the A_0 mode converts into an R wave, the amplitude of the R wave is low until 17 mm, after which the amplitude increases and stabilizes. A distance of 7 mm from the discontinuity can be taken as the generation distance for the R wave. This agrees well with the hypothesis that the diffraction from the discontinuity will combine with the grazing incidence, resulting in a generation length for the Rayleigh wave. For the case of the incident R mode, the numerical Ux line scan of $R \rightarrow A_0$ and S_0 conversion is shown in Figure 9b. After the discontinuity, the mode undergoes a resonance effect in space which results in an increase and a decrease in the amplitudes. The resonance effect can be explained by the difference in velocity of the Lamb modes and the constructive and destructive interference that results from the phase difference between the A_0 and S_0 modes. While there is no distinct diffraction effect for the case of $R \rightarrow A_0$ and S_0, the resonance effect will still result in a generation length for the Lamb modes. The resonance effects stops when overlap/superposition of A_0 and S_0 modes stops. From Figure 9b, it is apparent that this corresponds to a length of 33 mm after the defect. This generation length will also be a function of frequency and more work is required to understand this effect. It is important to note that in both cases, any power coefficient measurement in the region before the full generation occurs will result in erroneous transmission coefficient values.

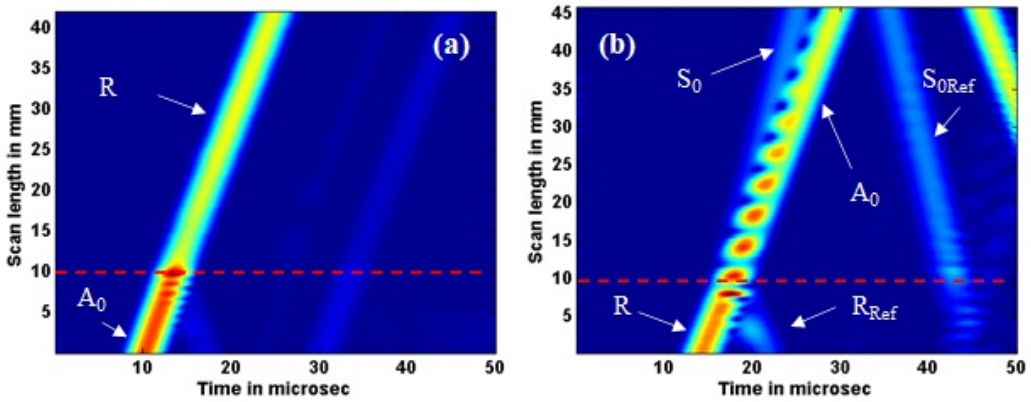

Figure 9. Numerical Hilbert B-Scans for (**a**) interaction of the A_0 mode with the discontinuity and A_0R generation and (**b**) incident R mode and mode conversion to RA_0 and RS_0.

Limitations and future work: The generation length results suggest that the position of the receiver when carrying out a measurement is significant. This is especially critical where characterization of the plate thickness is dependent on the measured transmission coefficients. Therefore, understanding the mode conversion phenomenon becomes critical for such NDE and SHM applications. The above-described hypotheses are all frequency dependent and require a more comprehensive analysis of different mode types and the effect of frequency on the mode conversion phenomenon. However, this is out of the scope of the current paper and will be explored elsewhere. The case of a plate attached to a half space can also be generalized to a rib as shown earlier [24]. The analysis carried out here has to be repeated for several combinations of plate thickness and frequency to confirm that the mode conversion phenomenon is conserved but the efficiency changes. The mode type and frequency dependence also need to be validated with experimental results.

In the case of Lamb to Rayleigh conversion, Figures 4 and 5 shows a Rayleigh wave propagating along the vertical edge. As mentioned earlier, this Rayleigh energy is included in a power coefficient analysis. From an NDE perspective, both waves are of interest. However, one application of the current problem is inspecting inaccessible structures, wherein the vertical edges may not be accessible from the outside. Additionally, the case

of a plate attached to a quarter space can be treated as an elastic wedge problem with the plate thickness $h \to 0$. In this case, it is important to address both Rayleigh modes as shown earlier [25]. Since the current work is only interested in understanding the Lamb–Rayleigh mode conversion, we limited the focus to the Rayleigh wave propagating along the horizontal edge.

5. Summary

The primary objective of this work was to understand mode conversion between Lamb and Rayleigh waves. Finite element models were used to study the mode conversions in a plate attached to a quarter space. The results suggest that the incident A_0 mode has a higher mode conversion efficiency compared to the incident S_0 mode. Two hypotheses were developed to explain this difference in mode conversion efficiency and tested using numerical models. The first hypothesis of the grazing incidence of bulk modes was studied numerically, and the results suggest that the incident A_0 mode has a higher SV component at grazing incidents on the stress-free boundary compared to the S_0 mode, which results in P waves at the grazing incidence. The grazing incidence of SV waves forms the basis for exponentially decaying waves, which confirms the hypothesis of a higher generation efficiency of the A_0 mode. The second hypothesis of generation length was also tested by carrying out numerical line scans. The results show that $A_0 \to R$ has a finite generation length, and $R \to A_0$ and S_0 results in a beat-like phenomenon.

There are several applications of this work, including nondestructive evaluation and structural health monitoring, where a plate attached to a quarter or half space can be used as a waveguide to generate L waves, which will mode convert and generate bulk and R modes. Mode conversions at steps, wedges and delaminations are also of interest to the NDE community and understanding the fundamental mode conversion is important for efficient NDE. The guided wave aspect of Lamb waves allows us to reach components that are not accessible using conventional methods. Therefore, understanding the mode conversion between these wave modes can help us to develop advanced inspection capabilities.

Author Contributions: A.V.: formal analysis, data curation, investigation, writing; L.J.B.: writing-review and editing, formal analysis; S.K.C.: formal analysis, investigation, writing-reivew and editing. All authors have read and agreed to the published version of the manuscript.

Funding: This research received no external funding.

Institutional Review Board Statement: Not applicable.

Informed Consent Statement: Not applicable.

Data Availability Statement: Data will be made available on request by contact Sunil K. Chakrapani.

Acknowledgments: The authors would like to acknowledge Vinay Dayal for many helpful discussions during the course of this research.

Conflicts of Interest: The authors declare no conflict of interest.

References

1. Auld, B.A. *Acoustic Fields and Waves in Solids*; Krieger Publishing Company: Malabar, FL, USA, 1973; Volume 2.
2. Rose, J.L. *Interface Waves*; Cambridge University Press: Cambridge, UK, 2004; pp. 132–135.
3. Graff, K.F. *Wave Motion in Elastic Solids*; Dover Publication, Inc: New York, NY, USA, 1975.
4. Cho, Y. Estimation of ultrasonic guided wave mode conversion in a plate with thickness variation. *IEEE Trans. Ultrason. Ferroelectr. Freq. Control.* **2000**, *47*, 591–603. [PubMed]
5. Cho, Y.; Rose, J.L. A boundary element solution for a mode conversion study on the edge reflection of Lamb waves. *J. Acoust. Soc. Am.* **1996**, *99*, 2097–2109. [CrossRef]
6. Han, J.; Kim, C.G.; Kim, J.Y. The propagation of Lamb waves in a laminated composite plate with a variable stepped thickness. *Compos. Struct.* **2006**, *76*, 388–396. [CrossRef]
7. Tuan, H.S.; Li, R.C.M. Rayleigh-wave reflection from groove and step discontinuities. *J. Acoust. Soc. Am.* **1974**, *55*, 1212–1217. [CrossRef]

8. Chang, C.P.; Tuan, H.S. On the surface-to-bulk mode conversion of Rayleigh waves. *IEEE Trans. Microw. Theory Tech.* **1973**, *21*, 558–560.
9. Blake, R.J.; Bond, L.J. Rayleigh wave scattering from surface features: Wedges and down-steps. *Ultrasonics* **1990**, *28*, 214–228. [CrossRef]
10. Saffari, N.; Bond, L.J. Body to Rayleigh wave mode-conversion at steps and slots. *J. Nondestruct. Eval.* **1987**, *6*, 1–22. [CrossRef]
11. Martel, L.; Munasinghe, M.; Farnell, G.W. Transmission and reflection of Rayleigh wave through a step. *Bull. Seismol. Soc. Am.* **1977**, *67*, 1277–1290. [CrossRef]
12. Darinskii, A.N.; Weihnacht, M.; Schmidt, H. Rayleigh wave scattering from a vertical edge of isotropic substrates. *Ultrasonics* **2014**, *54*, 1999–2005. [CrossRef] [PubMed]
13. Darinskii, A.N.; Weihnacht, M.; Schmidt, H. Mutual conversion of bulk and surface acoustic waves in gratings of finite length on half-infinite substrates. I. FE analysis of surface wave generation. *Ultrasonics* **2013**, *53*, 998–1003. [CrossRef] [PubMed]
14. Shkerdin, G.; Glorieux, C. Lamb mode conversion in a plate with a delamination. *J. Acoust. Soc. Am.* **2004**, *116*, 2089–2100. [CrossRef]
15. Chakrapani, S.K.; Dayal, V. The interaction of Rayleigh waves with delaminations in composite laminates. *J. Acoust. Soc. Am.* **2014**, *135*, 2646–2653. [CrossRef] [PubMed]
16. Schaal, C.; Samajder, H.; Baid, H.; Mal, A. Rayleigh to Lamb wave conversion at a delamination-like crack. *J. Sound Vib.* **2015**, *353*, 150–163. [CrossRef]
17. Achenbach, J.D.; Lin, W.; Keer, L.M. Surface waves due to scattering by a near-surface parallel crack. *IEEE Trans. Sonics Ultrason.* **1983**, *30*, 270–276. [CrossRef]
18. Newmark, N.M. A method of computation for structural dynamics. *J. Eng. Mech. Div.* **1959**, *85*, 67–94. [CrossRef]
19. Krawezik, G.P.; Poole, G. Accelerating the ANSYS direct sparse solver with GPUs. In Proceedings of the Symposium on Application Accelerators in High Performance Computing, SAAHPC, Urbana, IL, USA, 28–30 July 2009 .
20. Graczykowski, B. The reflection of Rayleigh surface waves from single steps and grooves. *J. Appl. Phys.* **2012**, *112*, 103520. [CrossRef]
21. Simons, D.A. Scattering of normally incident Rayleigh waves by thin strips. *J. Acoust. Soc. Am.* **1976**, *60*, 1100–1107. [CrossRef]
22. Richart, F.E.; Hall, J.R.; Woods, R.D. *Vibrations of Soils and Foundations*; Prentice-Hall, Inc.: Hoboken, NJ, USA, 1970.
23. Goodier, J.N.; Bishop, R.E.D. A note on critical reflections of elastic waves at free surfaces. *J. Appl. Phys.* **1952**, *23*, 124–126. [CrossRef]
24. Bond, L.; Taylor, J. Interaction of Rayleigh waves with a rib attached to a plate. *Ultrasonics* **1991**, *29*, 451–458. [CrossRef]
25. Gautesen, A. Scattering of a Rayleigh wave by an elastic wedge whose angle is less than 180. *Wave Motion* **2002**, *36*, 417–424. [CrossRef]